

Chapter

Machine Learning Architectures and Their Applications in Optical Coherence Tomography

Ankit Butola

Abstract

Optical coherence tomography (OCT) is a powerful imaging technique that utilizes optical scattering to extract tomographic information of biological samples in their natural state. Over the past two decades, OCT has advanced both experimentally and computationally to improve its performance in terms of resolution, penetration depth, acquisition speed, and sensitivity. The interpretability of OCT particularly increased through its integration with artificial intelligence (AI). While fast and label-free nature of OCT becomes popular in optical imaging, AI assigned an artificial system to mimic human intelligence, such as classification, visualizations, and segmentation. In particular, the subfield of AI, i.e., machine learning (ML) is a data-driven approach, which is explicitly designed and optimized by fine-tuning the hyperparameters to reflect certain features through learning rule. In this chapter, we aim to provide a critical overview of OCT and machine learning model by presenting the scientific context, working principles, and current biomedical applications. The chapter will also cover types of convolutional neural networks (CNNs) that have been used in analyzing diverse OCT images.

Keywords: optical coherence tomography, optical microscopy, machine learning, deep neural network, ophthalmology, classification, segmentation

1. Introduction

Optical coherence tomography (OCT) is a non-contact and non-invasive optical technique to visualize the volumetric information of multilayered semitransparent objects [1, 2]. OCT is based on the principle of low-coherence interferometry (LCI) [1, 2]. There are different types of OCT techniques described in the literature that can provide volumetric information of the object, such as Time-Domain OCT (TD-OCT), Frequency Domain OCT (Spectral Domain OCT and Swept-Source OCT (SS-OCT)), and Full-Field OCT (FF-OCT) [1, 3]. In general, two types of scans must be performed in OCT to acquire the volumetric information of the specimen: the lateral-scan, which is performed by galvo scan, addresses laterally adjacent sample positions and the depth-scan to detect the depth information of the sample [4, 5]. In addition, the axial resolution of OCT is determined by the coherence length (l_c) of the light source rather than the depth of field of the objective lens.

OCT has found widespread use in ophthalmology, cardiology, dermatology, among other fields due to its ability to provide detailed cross-sectional images of tissue structures with micrometer resolution [5, 6]. The penetration depth of several millimeters in industrial sample and 1–2 mm in tissue makes it most suitable for the diverse biological applications [7, 8]; 1–2 mm of depth of penetration of OCT is primarily decided by the cellular and subcellular density. This penetration depth of 1–2 mm is helpful in many applications, for example, surgeon to anticipate tissue morphology beneath the surface and over large surface areas while conserving the tissue structure. In addition, it emerged as a gold standard technique for early diagnosis of retinal disease [3]. It provides cross-sectional images of the retina and optic nerve that enable early stage diagnosis and used to monitor conditions, such as macular degeneration, diabetic retinopathy, and glaucoma [9]. Over the last three decades, OCT has been developed both experimentally and computationally to improve its resolution, acquisition speed, depth of penetration, and therefore strengthen its applicability in various biological and biomedical applications [10, 11].

In recent years, the integration of artificial intelligence (AI) with OCT revolutionized its applicability in biophotonics [12–14]. AI has made remarkable progress in various domains that include image processing, natural language processing, autonomous systems, among others [15, 16]. The fast and label-free nature of OCT combined with the data analysis capabilities of machine learning brings forth systems that can mimic human intelligence, performing tasks, such as classification, virtual staining, identification of hidden features, and segmentation of objects [17, 18]. Machine learning involves the design and optimization of models through hyperparameter tuning that allow to extract specific features via learning rules [16, 19].

The application of machine learning to OCT has led to significant improvements in image interpretation, noise reduction, and feature extraction. Various machine learning techniques, such as supervised learning, unsupervised learning, and reinforcement learning, have been employed to enhance the performance of OCT systems [7]. For example, supervised learning models like support vector machines (SVMs) and random forests have been used to classify ocular diseases and breast cancer [20]. Unsupervised learning methods, such as K-means clustering and Principal Component Analysis (PCA), have been applied to segment images and identify patterns in large datasets [21].

Deep learning (DL), which is a subset of machine learning, has emerged as a powerful tool in the analysis of OCT images. Convolutional neural networks (CNNs) and recurrent neural networks (RNNs) are two prominent architectures that have shown significant promise in this area. CNNs with their ability to automatically learn hierarchical features from raw image data have been widely used for tasks, such as image classification, segmentation, and resolution enhancement [22, 23]. For instance, CNNs have been applied to identify pathological features in retinal OCT images, achieving high accuracy and robustness. RNNs, which are well suited for sequential data, have been utilized to analyze time-series OCT data, enabling dynamic tracking of changes in tissue morphology.

For example, AI-driven OCT systems can provide real-time diagnostic support to clinicians, aiding in the early detection and treatment of diseases. Furthermore, the ability to process and analyze large-scale OCT datasets with AI can lead to the discovery of novel biomarkers and therapeutic targets. The synergy between OCT and AI is also fostering advancements in personalized medicine, where imaging data can be used to tailor treatments to individual patients.

This chapter covers fundamental principles of OCT and machine learning models utilized for interpreting OCT images. It explores the foundational aspects of supervised

and unsupervised learning models, along with advanced deep learning architectures, such as CNNs and RNNs. In addition, various applications of conventional and modern machine learning architectures are shown for the classifications and segmentation of OCT images. In addition to discussing the technical aspects of machine learning models, this chapter also addresses the practical considerations for implementing AI in OCT systems. The goal is to provide a comprehensive overview of the current state of AI in OCT and a roadmap for future research and development.

2. Principle of optical coherence tomography

OCT is based on the principle of low-coherence interferometry (LCI) [1, 2]. The experimental setup of LCI is shown in **Figure 1**. Light from a low-coherence (broad-band) source is incident on the sample surface through the Michelson interferometer [24]. The light is split into reference and sample beams using 50:50 beam splitter. At each scan point, the back-scattered light intensity from multiple layers of the sample combines with the back-reflected light from the reference mirror to generate a 1D (one-dimensional) interference signal only when the optical path difference between two arms is less than the coherence length of the light source [1, 25]. The encoded depth information in the detected interference signal is reconstructed using Fourier transform analysis.

If $E_r = \frac{E_i}{\sqrt{2}} r_{ref} e^{i2kz_r}$ and $E_s = \frac{E_i}{\sqrt{2}} \sum_{n=1}^N r_{Sn} e^{i2kz_{sn}}$ represent the electric fields at the beam splitter after reflecting from reference and nth layer of the sample arm, respectively, the 1D interference signal at the detector can be written as

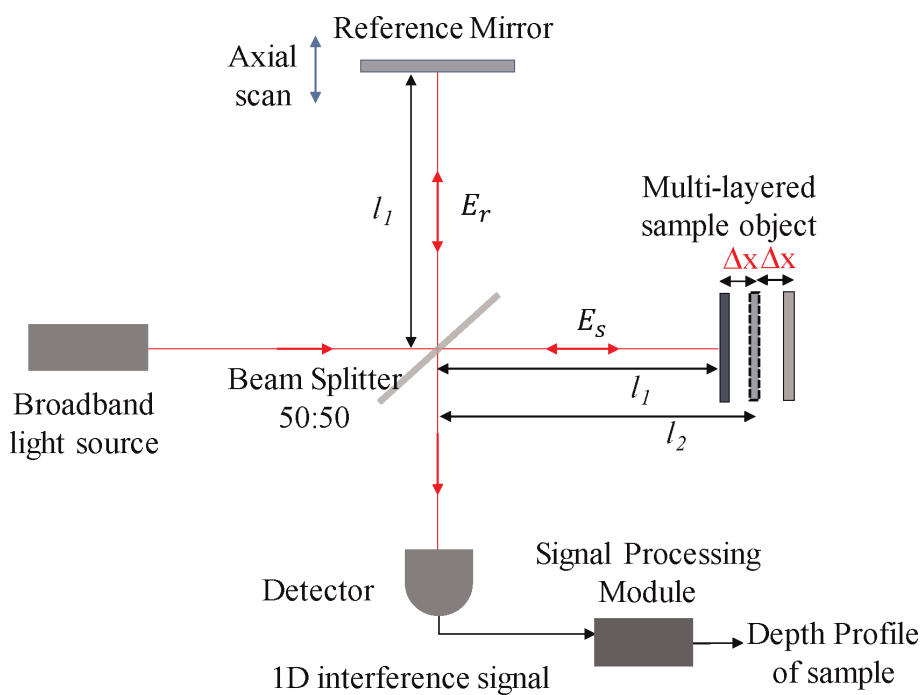


Figure 1.
Schematic diagram of low-coherence interferometry.

$$I(k, w) = \frac{\mu}{2} \left\langle \left| \frac{s(k, w)}{\sqrt{2}} r_{ref} e^{i(2kz_r - wt)} + \frac{s(k, w)}{\sqrt{2}} \sum_{n=1}^N r_{Sn} e^{i(2kz_{sn} - wt)} \right|^2 \right\rangle \quad (1)$$

where $s(k, w)$ represents the electric field amplitude and μ is the responsivity of the detector (Amperes/Watts). r_{ref} and r_{Sn} show the electric field reflectivity of the reference and nth layer of the sample arm, respectively. The above equation can be expanded as

$$\begin{aligned} I(k, w) &= \frac{\mu}{4} [S(k)(R_{ref} + R_{s1} + R_{s2} + \dots + R_{sn})] \\ &\quad + \frac{\mu}{2} \left[S(k) \sum_{n=1}^N \sqrt{R_{ref} R_{sn}} (e^{i2k(z_{ref} - z_{sn})} + e^{-i2k(z_{ref} - z_{sn})}) \right] \\ &\quad + \frac{\mu}{4} \left[S(k) \sum_{n \neq m=1}^N \sqrt{R_{sn} R_{sn}} (e^{i2k(z_{sm} - z_{sn})} + e^{-i2k(z_{sm} - z_{sn})}) \right] \end{aligned} \quad (2)$$

The above equation can be rewritten as

$$\begin{aligned} I(k, w) &= \frac{\mu}{4} [S(k)(R_{ref} + R_{s1} + R_{s2} + \dots + R_{sn})] \\ &\quad + \frac{\mu}{2} \left[S(k) \sum_{n=1}^N \sqrt{R_{ref} R_{sn}} (2\cos(2k(z_{ref} - z_{sn})) \right] \\ &\quad + \frac{\mu}{4} \left[S(k) \sum_{n \neq m=1}^N \sqrt{R_{sn} R_{sn}} (2\cos(2k(z_{sm} - z_{sn})) \right] \end{aligned} \quad (3)$$

Here, $S(k)$ represents Gaussian spectral profile i.e. square of the electric field amplitude encodes the spectral dependence of the light source. In addition, the degree of coherence for a light source with Gaussian spectral profile is given by

$$\gamma(\tau) = \exp \left[- \left(\frac{\pi \Delta \nu \tau}{2 \sqrt{\ln 2}} \right)^2 \right] \cdot \exp(-j2\pi\nu_0\tau) \quad (4)$$

where $\Delta\nu$ is the width of the temporal frequency spectrum and ν_0 is the central frequency of the light source. The key point in OCT imaging system is the dominance of coherence function over axial point-spread function (at least for low numerical aperture lens); hence, the axial resolution of OCT system is defined by the coherence length of the light source [26].

An especial type of OCT is called SD-OCT, where the reflectivity of the sample can be calculated by taking the inverse Fourier transform of Eq. (2), mathematically

$$\begin{aligned} IFT[I(k, w)] &= IFT \left[\frac{\mu}{4} [S(k)(R_{ref} + R_{s1} + R_{s2} + \dots + R_{sn})] \right. \\ &\quad \left. + \frac{\mu}{2} \left[S(k) \sum_{n=1}^N \sqrt{R_{ref} R_{sn}} (e^{i2k(z_{ref} - z_{sn})} + e^{-i2k(z_{ref} - z_{sn})}) \right] \right. \\ &\quad \left. + \frac{\mu}{4} \left[S(k) \sum_{n \neq m=1}^N \sqrt{R_{sn} R_{sn}} (e^{i2k(z_{sm} - z_{sn})} + e^{-i2k(z_{sm} - z_{sn})}) \right] \right] \end{aligned} \quad (5)$$

Since cosine and delta functions are Fourier transform pair of each other, the above equation can be simplified as:

$$\begin{aligned} I(z) = & \frac{\mu}{8} [\gamma(z)(R_{ref} + R_{s1} + R_{s2} + \dots R_{sn})] \\ & + \frac{\mu}{4} \left[\gamma(z) \otimes \sum_{n=1}^N \sqrt{R_{ref}R_{sn}} (\delta(z \pm 2(z_{ref} - z_{sn}))) \right] \\ & + \frac{\mu}{8} \left[\gamma(z) \otimes \sum_{n \neq m=1}^N \sqrt{R_{sn}R_{sn}} (\delta(z \pm 2(z_{sm} - z_{sn}))) \right] \end{aligned} \quad (6)$$

where $[\gamma(z)(R_{ref} + R_{s1} + R_{s2} + \dots R_{sn})]$ is the “DC term,” $\frac{\mu}{8} \left[\gamma(z) \otimes \sum_{n=1}^N \sqrt{R_{ref}R_{sn}} (\delta(z \pm 2(z_{ref} - z_{sn}))) \right]$ represents the “auto-correlation term” i.e. correlation between nth and nth layer of the sample. Additionally, $\frac{\mu}{4} \left[\gamma(z) \otimes \sum_{n=1}^N \sqrt{R_{ref}R_{sn}} (\delta(z \pm 2(z_{ref} - z_{sn}))) \right]$ shows the “cross-correlation term” where desired sample field reflectivity i.e. $\sqrt{R_s(z_s)}$ is correlated with the reference field. Using the sifting property of the delta function i.e.

$$\gamma(z) \otimes \delta(z - z_0) = \gamma(z - z_0) \quad (7)$$

Eq. (11) referred to as “A-scan” can be written as

$$\begin{aligned} I(z) = & \frac{\mu}{8} [\gamma(z)(R_{ref} + R_{s1} + R_{s2} + \dots R_{sn})] \\ & + \frac{\mu}{4} \left[\sum_{n=1}^N \sqrt{R_{ref}R_{sn}} [\gamma[2(z_{ref} - z_{sn})] + \gamma[-2(z_{ref} - z_{sn})]] \right] \\ & + \frac{\mu}{8} \left[\sum_{n \neq m=1}^N \sqrt{R_{sn}R_{sn}} [\gamma[2(z_{sm} - z_{sn})] + \gamma[-2(z_{sm} - z_{sn})]] \right] \end{aligned} \quad (8)$$

SD-OCT has a dramatic sensitivity and speed advantage because depth-scan is not required. It also allows direct access to the spectrum, which enables numerical dispersion compensation and spectral shaping.

3. The necessity of machine learning for OCT image interpretation

Although OCT is a powerful label-free, non-invasive technique, the interpretation of OCT images poses several challenges. First, chemical specificity of OCT images is limited compared to the label-based imaging methods such as fluorescence microscopy. The primary bottleneck comes with mapping chemical composition with the OCT image of the object. Second, high-dimensional data produced by OCT scans can be overwhelming, making manual analysis time-consuming and prone to errors. Finally, subtle features indicative of early-stage diseases can be easily overlooked by the human eye. Therefore, traditional image analysis techniques often fall short of effectively distinguishing between fine structures and artifacts or noise, limiting the diagnostic utility of OCT.

Machine learning offers powerful solutions to these challenges. Modern deep learning models, such as convolutional neural networks (CNNs), are designed to automatically learn and extract hierarchical features from raw image data [27]. These models can be trained on large datasets of labeled OCT images to recognize patterns and structures associated with specific biological or pathological states. By doing so, machine learning algorithms can perform tasks, such as multilayer/object-specific segmentation, disease detection, and classification.

For example, machine learning models can analyze OCT images to segment retinal layers, detect fluid accumulation, and identify biomarkers for diseases like age-related macular degeneration, drusen, and diabetic retinopathy. These algorithms can also adapt to variations in image quality and patient-specific differences, providing robust and generalized solutions. Therefore, machine learning can bridge the technical gap by leveraging its ability to learn from data, automatically extract relevant features, and provide accurate and consistent analysis, thereby enhancing the diagnostic and research capabilities of OCT in biomedical applications.

4. Convolutional neural network

Convolutional neural networks (CNNs) consist of several types of layers, including convolutional layers, max-pooling layers, rectified linear unit (ReLU) layers, and fully connected layers followed by a soft-max layer for classification purposes [15].

Figure 2 illustrates the architecture of CNNs. The learning process begins by applying a convolution operation to the input image using the filters in the first convolutional layer.

In general, convolution is an operation between two functions, f and k , which produces third function ‘ s ’ that represents the modification of the shape of one function by the other. Mathematically, this is expressed as:

$$s(t) = \int f(x)k(t-x) dx \quad (9)$$

For a 2D (two-dimensional) image, f of size $M \times N$ and a 2d kernel k of size $m \times n$, the convolution operation is given by:

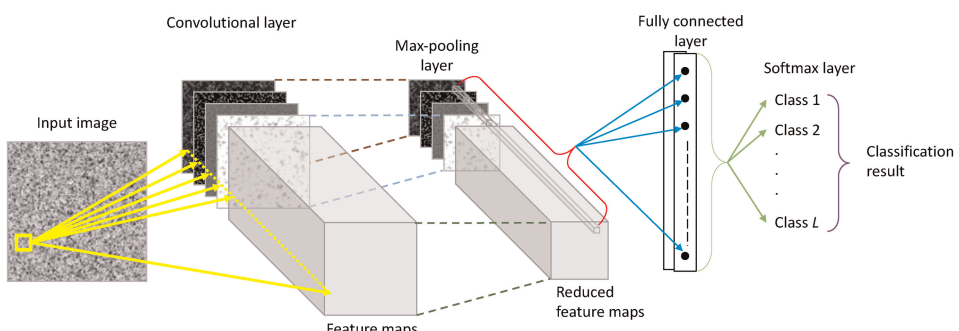


Figure 2.

Schematic diagram of convolutional neural network consisting of convolutional layer, max-pooling layer, fully connected layer, and soft-max layer.

$$s(i,j) = \sum_{a=0}^{m-1} \sum_{b=0}^{n-1} f(i+a, j+b) \bullet k(a, b) \quad (10)$$

This can be generalized for color images, where the convolution is performed across each channel.

$$s(i,j,c) = \sum_{a=0}^{m-1} \sum_{b=0}^{n-1} \sum_{d=0}^{D-1} f(i+a, j+b, d) k(a, b, c, d) \quad (11)$$

where D is the depth of the input image (number of channels) and c is the output channel.

To control the spatial dimensions of the output, padding and stride are used. Padding p involves usually adding zeros around the input image and stride s controls the step size of the convolution.

For a given input f of size $M \times N$ and a kernel k of size $m \times n$, with padding p and stride s , the output size (M', N') is calculated as:

$$M' = \left(\frac{M - m + 2p}{s} \right) + 1 \quad (12)$$

$$N' = \left(\frac{N - n + 2p}{s} \right) + 1 \quad (13)$$

Furthermore, ReLU activation function introduces non-linearity to the network, which is crucial for learning complex patterns. Mathematically, it can be defined as:

$$f(x) = \max(0, x) \quad (14)$$

Max-pooling operation followed the ReLU layer, which reduces the spatial dimensions while retaining the most critical information. For an input feature map f and a pooling window of size $m \times n$, the max-pooling operation is given by:

$$f_{i,j} = \max \{f(i+a, j+b) | 0 \leq a < m, 0 \leq b < n\} \quad (15)$$

Furthermore, the fully connected layer aggregated the features extracted by previous layers to make the final prediction. It is represented as:

$$z = W \bullet x + b \quad (16)$$

where W is the weight matrix, x is the input vector, and b is the bias vector. Finally, the SoftMax function converts the raw scores from the fully connected layer into probabilities:

$$\text{softmax}(z_i) = \frac{e^{z_i}}{\sum_j e^{z_j}} \quad (17)$$

This ensures that the output probabilities sum to 1. The convolutional neural network combines multiple convolutional layers, each followed by ReLU and max-pooling layers, to learn spatial hierarchies of features. The fully connected layer then integrates these features to classify the input data accurately. Understanding these

mathematical formulations can help to grasp how CNNs effectively process and interpret complex image data, such as those produced by OCT.

5. Machine learning approach for the analysis of OCT images

Table 1 provides the systematic review of different types of OCT techniques that have been used to acquire 3D images of different biological samples. These images are used by different machine learning methods for specific biological applications.

In the past two decades, various types of OCT techniques have been used for various biological applications where machine learning plays a pivotal role in data analysis and

OCT techniques	Biological sample	ML method	Key findings
SD-OCT	Retinal tissue [3, 9, 28, 29]	Convolutional neural networks (CNNs)	Classification of retinal diseases
		Support vector machine (SVM)	Detection of diabetic retinopathy
SS-OCT	Corneal tissue [20, 30, 31]	Support vector machine (SVM)	Detection of keratoconus
		Random forest	Classification of corneal diseases
Doppler OCT	Blood flow in retinal vessels [21, 32, 33]	Random forest	Analysis of blood flow dynamics
		K-means clustering	Segmentation of blood vessels
	Cardiovascular tissues [34]	CNNs	Detection of myocardial infarction
Polarization-Sensitive OCT	Liver tissues [35]	CNNs	Detection of hepatic microvasculature
	Skin tissue [23, 36]	Principal component analysis (PCA)	Assessment of burn depth
Time-Domain OCT (TD-OCT)		K-means clustering	Differentiation of skin layers
Dental tissue [37]	k-Nearest Neighbors (k-NN)	Detection of dental caries	
Full-Field OCT (FF-OCT)	Brain tissue [38, 39]	Linear discriminant analysis (LDA)	Imaging of neural structures
		SVM	Classification of brain tissue
OCT Angiography (OCTA)	Retinal vasculature [22, 40]	CNNs	Visualization of microvascular networks
			Automated segmentation of retinal layers
Multi-Modal OCT	Tumor tissue [41, 42]	Ensemble methods	Differentiation of tumor margin
		Random forest	Classification of tumor types

Table 1.

Detailed review of different types of OCT techniques and machine learning models that have been used to extract and analyze 3D images of diverse biological samples.

interpretation. For instance, Spectral-Domain OCT (SD-OCT) has been extensively applied in ophthalmology, particularly for imaging retinal tissues [3, 9, 28, 29]. Advance machine learning (ML) techniques, such as CNN and support vector machines (SVMs), assisted SD-OCT for automated classification of retinal diseases like diabetic retinopathy, drusen, etc. These algorithms analyze OCT images to detect multilayer structural changes, providing clinicians with accurate diagnostic information [29].

Another type of OCT technique i.e., Swept-Source OCT (SS-OCT) has been extensively used for retinal imaging due to its high-resolution and rapid acquisition capabilities [20, 30, 31]. CNNs significantly improved the classification of retinal diseases, such as diabetic retinopathy and age-related macular degeneration, by automatically identifying disease-specific patterns in OCT images. SS-OCT also offers deeper tissue penetration, making it suitable for imaging the cornea. Studies have used SVMs to detect keratoconus, a degenerative corneal disorder, with improved accuracy by analyzing the curvature and thickness of the corneal layers. Additionally, Random Forest algorithms have been applied to classify various corneal diseases, enhancing diagnostic precision.

On the other hand, researchers also used Doppler OCT to measure blood flow velocity and analyze retinal blood flow dynamics [21]. Different ML techniques, such as Random Forest algorithms, have facilitated the segmentation and analysis of blood vessels, providing insights into conditions like glaucoma and diabetic retinopathy. K-means clustering has also been employed for vessel segmentation, enhancing the visualization of retinal vasculature. Doppler OCT has also been applied to liver tissues for the assessment of fibrosis and detection of hepatic microvasculature, using Random Forest and CNN algorithms.

Polarization-Sensitive OCT (PS-OCT), which provides additional contrast based on tissue birefringence, has been used for assessing burn depth and differentiating skin layers [23, 36]. Principal Component Analysis (PCA) has been utilized to quantify changes in birefringence, aiding in the assessment of burn injuries. K-means clustering has helped in differentiating various skin layers, facilitating detailed structural analysis.

Time-Domain OCT (TD-OCT) has also been applied to dental imaging for the detection of dental caries [37]. Techniques like k-Nearest Neighbors (k-NN) have been employed to classify carious and non-carious regions, leveraging the detailed structural information provided by TD-OCT. Decision Trees have also been used to analyze dental tissues, aiding in the diagnosis and treatment planning.

For en face imaging, Full-Field OCT (FF-OCT) is explored to extract high-resolution imaging of neural structures in brain tissue [21]. Linear Discriminant Analysis (LDA) has facilitated the differentiation of various neural structures, aiding in neurological research. SVMs have also been applied to classify different types of brain tissues, providing valuable insights for neuroscientific studies.

Furthermore, detailed imaging of retinal microvascular networks is explored by using OCT Angiography (OCTA) [22, 40]. DL methods have been employed to automate the segmentation and visualization of these networks, enhancing the detection and monitoring of diseases, such as macular degeneration and diabetic retinopathy. Finally, Multi-Modal OCT combines various OCT techniques to provide comprehensive imaging of tumor tissues. Ensemble methods and Random Forest algorithms have been used to differentiate tumor margins and classify tumor types, improving the precision of oncological diagnoses.

The integration of OCT techniques with advanced machine learning methods has revolutionized its applicability for biological imaging. By leveraging the strengths of both technologies, researchers and clinicians can achieve more accurate diagnoses, better disease monitoring, and deeper insights into complex biological processes. The

extensive range of applications highlighted in **Table 1** underscores the versatility and potential of combining OCT with machine learning in various domains of biological research and medical practice.

6. Practical prescription for machine learning in OCT images

A careful examination must be required to ensure accurate outcomes of using ML in OCT images. These challenges include technical, computation, and practical aspects of the integration of ML with OCT datasets.

For instance, OCT images often contain noise and artifacts due to the multiple components in the optical system, scanning, sample movement, and external vibrations. These artifacts can significantly affect the image quality and registration, as a consequence, can complicate the training process of ML models. Furthermore, establishing a reliable ground truth is critical for training and validation of ML models. Inconsistency in the ground truth labeling can lead to unreliable results and poor performance of the model. In addition, overfitting and underfitting are the common causes of training/testing failures. Such issues can be avoided by the appropriate

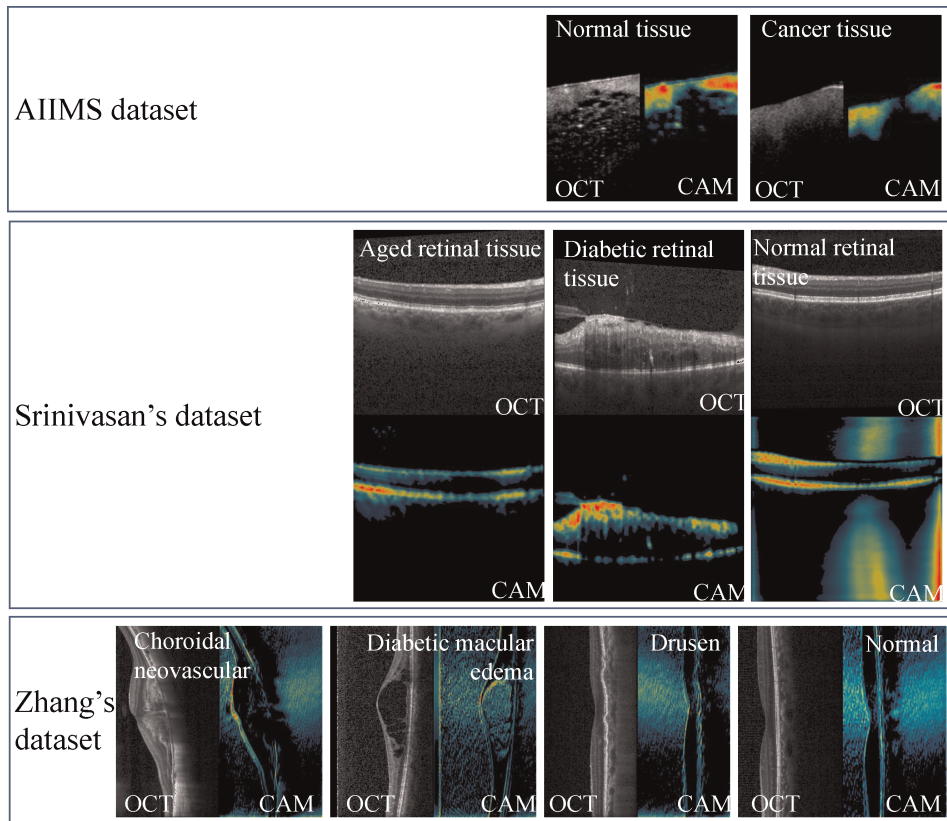


Figure 3.

OCT images (a_1-i_1) and class activation maps (CAMs) (a_2-i_2) to highlight the regions of an input image that are most relevant for predicting a specific class. OCT and CAMs images of normal/cancerous breast cancer tissue (All India Institute of Medical Sciences datasets) and ocular disease (Srinivasan and Zhang datasets) OCT images [9, 31, 44].

choice of ML models, and tuning the model's hyperparameters (such as the number of layers and learning rate).

Furthermore, visualization in deep learning is important to highlight the regions of an input image that are most relevant for predicting a specific class. Class activation maps (CAMs) help interpret and understand the decision-making process of CNNs by indicating which parts of the image contribute most to the network's final classification decision [43]. CAMs (see **Figure 3**) represent the firing strength of various regions that help in the conclusion regarding the class label [45]. For objects with well-defined boundaries in both the training and test datasets, researchers have employed activation maps to explore and interpret the behavior of CNN models. By visualizing the areas of an image that contribute most to the network's classification, CAMs help bridge the gap between complex neural network operations and interpretability.

7. Conclusion

Optical Coherence Tomography (OCT) combined with machine learning offers a powerful tool for the automated classification of biological samples into diagnostically relevant classes. OCT is a promising, label-free imaging technique that provides volumetric information, offering advantages over conventional label-free methods. In the future, fully automated classification using OCT and machine learning can serve as a valuable intermediate tool for experts across multiple medical applications, including ophthalmology and to distinguish between normal and abnormal tissues.

Furthermore, deep learning-based methods for classification, segmentation, virtual staining, and resolution enhancement hold broad applications in biomedical imaging. These data-driven approaches can improve the robustness, reduce computational artifacts, and enhance selectivity and sensitivity in optical imaging. However, it is crucial to be aware of the limitations of AI in biomedical imaging to fully understand the potential benefits of data-driven learning. Therefore, machine learning models must undergo rigorous validation to meet regulatory standards for clinical use. Ensuring that these models are reliable, safe, and effective across diverse clinical environments is essential for achieving regulatory approval. By overcoming practical challenges and integrating machine learning with OCT can enhance diagnostic accuracy, improve patient outcomes, and drive advancements in the field of biomedical imaging.

Acknowledgements

The author would like to acknowledge the European Research Council Starting Grant (ID 804233).

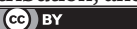
Author details

Ankit Butola

Department of Physics and Technology, UiT The Arctic University of Norway,
Tromsø, Norway

*Address all correspondence to: ankit.butola@uit.no; ankitbutola321@gmail.com

IntechOpen

© 2025 The Author(s). Licensee IntechOpen. This chapter is distributed under the terms of the Creative Commons Attribution License (<http://creativecommons.org/licenses/by/4.0/>), which permits unrestricted use, distribution, and reproduction in any medium, provided the original work is properly cited. 

References

- [1] Drexler W, Fujimoto JG. Optical Coherence Tomography: Technology and Applications. Berlin, Heidelberg: Springer; 2008
- [2] Huang D, Swanson EA, Lin CP, Schuman JS, Stinson WG, Chang W, et al. Optical coherence tomography. *Science*. 1991;254:1178-1181
- [3] Lee CS, Baughman DM, Lee AY. Deep learning is effective for classifying normal versus age-related macular degeneration OCT images. *Ophthalmology Retina*. 2017;1: 322-327
- [4] Boppart SA. Optical coherence tomography. In: Optical Imaging and Microscopy: Techniques and Advanced Systems. Berlin, Heidelberg: Springer; 2003. pp. 309-337
- [5] Welzel J. Optical coherence tomography in dermatology: A review. *Skin Research and Technology*. 2001;7:1-9
- [6] De Carlo TE, Romano A, Waheed NK, Duker JS. A review of optical coherence tomography angiography (OCTA). *International Journal of Retina and Vitreous*. 2015;1:1-15
- [7] Joshi D, Butola A, Kanade SR, Prasad DK, Mithra SA, Singh N, et al. Label-free non-invasive classification of rice seeds using optical coherence tomography assisted with deep neural network. *Optics & Laser Technology*. 2021;137:106861
- [8] Mehta DS, Butola A, Singh V. Quantitative Phase Microscopy and Tomography: Techniques Using Partially Spatially Coherent Monochromatic Light. Bristol, United Kingdom: IOP Publishing; 2022
- [9] Kermany DS, Goldbaum M, Cai W, Valentim CC, Liang H, Baxter SL, et al. Identifying medical diagnoses and treatable diseases by image-based deep learning. *Cell*. 2018;172:1122-1131. e1129
- [10] Fujimoto JG. Optical coherence tomography for ultrahigh resolution *in vivo* imaging. *Nature Biotechnology*. 2003;21:1361-1367
- [11] Butola A, Coucheron DA, Szafranska K, Ahmad A, Mao H, Tinguely J-C, et al. Multimodal on-chip nanoscopy and quantitative phase imaging reveals the nanoscale morphology of liver sinusoidal endothelial cells. *Proceedings of the National Academy of Sciences*. 2021;118:e2115323118
- [12] Maloca PM, Lee AY, de Carvalho ER, Okada M, Fasler K, Leung I, et al. Validation of automated artificial intelligence segmentation of optical coherence tomography images. *PLoS One*. 2019;14:e0220063
- [13] Lee CS, Tyring AJ, Wu Y, Xiao S, Rokem AS, DeRuyter NP, et al. Generating retinal flow maps from structural optical coherence tomography with artificial intelligence. *Scientific Reports*. 2019;9:5694
- [14] Dubey K, Singla N, Butola A, Lathe A, Quaiser D, Srivastava A, et al. Ensemble classifier for improve diagnosis of the breast cancer using optical coherence tomography and machine learning. *Laser Physics Letters*. 2019;16:025602
- [15] Bengio Y, Goodfellow I, Courville A. Deep Learning. Cambridge, MA, USA: MIT press; 2017
- [16] LeCun Y, Bengio Y, Hinton G. Deep learning. *Nature*. 2015;521:436-444

- [17] Butola A, Popova D, Prasad DK, Ahmad A, Habib A, Tinguely JC, et al. High spatially sensitive quantitative phase imaging assisted with deep neural network for classification of human spermatozoa under stressed condition. *Scientific Reports.* 2020;10:13118
- [18] Butola A, Kanade SR, Bhatt S, Dubey VK, Kumar A, Ahmad A, et al. High space-bandwidth in quantitative phase imaging using partially spatially coherent digital holographic microscopy and a deep neural network. *Optics Express.* 2020;28:36229-36244
- [19] Zuo C, Qian J, Feng S, Yin W, Li Y, Fan P, et al. Deep learning in optical metrology: A review. *Light: Science & Applications.* 2022;11:1-54
- [20] Butola A, Ahmad A, Dubey V, Srivastava V, Qaiser D, Srivastava A, et al. Volumetric analysis of breast cancer tissues using machine learning and swept-source optical coherence tomography. *Applied Optics.* 2019;58:A135-A141
- [21] Mariampillai A, Standish BA, Moriyama EH, Khurana M, Munce NR, Leung MK, et al. Speckle variance detection of microvasculature using swept-source optical coherence tomography. *Optics Letters.* 2008;33:1530-1532
- [22] Kashani AH, Lee SY, Moshfeghi A, Durbin MK, Puliafito CA. Optical coherence tomography angiography of retinal venous occlusion. *Retina.* 2015;35:2323-2331
- [23] Marvdash T, Duan L, Aasi SZ, Tang JY, Bowden AKE. Classification of basal cell carcinoma in human skin using machine learning and quantitative features captured by polarization sensitive optical coherence tomography.
- Biomedical Optics Express. 2016;7:3721-3735
- [24] Usmani K, Ahmad A, Joshi R, Dubey V, Butola A, Mehta DS. Relationship between the source size at the diffuser plane and the longitudinal spatial coherence function of the optical coherence microscopy system. *JOSA A.* 2019;36:D41-D46
- [25] Butola A, Joshi T, Ahmad A, Dubey V, Senthilkumaran P, Mehta DS. 3D topography and tomography of multilayered freeform optical surfaces using large-range measurement swept-source low-coherence interferometry. *Laser Physics.* 2018;28:116101
- [26] Qin Y, Butola A, Agarwal K. 3D refractive index reconstruction from phaseless coherent optical microscopy data using multiple scattering-based inverse solvers—A study. *Inverse Problems.* 2023;40:015003
- [27] Jo Y, Cho H, Lee SY, Choi G, Kim G, Min H-S, et al. Quantitative phase imaging and artificial intelligence: A review. *IEEE Journal of Selected Topics in Quantum Electronics.* 2018;25:1-14
- [28] Archana R, Rajalakshmi T, Vijay Sai P. Non-invasive technique to detect diabetic retinopathy based on electrooculography signal using machine learning classifiers. *Proceedings of the Institution of Mechanical Engineers, Part H: Journal of Engineering in Medicine.* 2022;236:882-895
- [29] Abramoff MD, Fort PE, Han IC, Jayasundera KT, Sohn EH, Gardner TW. Approach for a clinically useful comprehensive classification of vascular and neural aspects of diabetic retinal disease. *Investigative Ophthalmology & Visual Science.* 2018;59:519-527

- [30] Tan O, Li G, Lu AT-H, Varma R, Huang D, A. I. f. G. S. Group. Mapping of macular substructures with optical coherence tomography for glaucoma diagnosis. *Ophthalmology*. 2008;115: 949-956
- [31] Butola A, Prasad DK, Ahmad A, Dubey V, Qaiser D, Srivastava A, et al. Deep learning architecture “LightOCT” for diagnostic decision support using optical coherence tomography images of biological samples. *Biomedical Optics Express*. 2020;11:5017-5031
- [32] Mariampillai A, Leung MK, Jarvi M, Standish BA, Lee K, Wilson BC, et al. Optimized speckle variance OCT imaging of microvasculature. *Optics Letters*. 2010;35:1257-1259
- [33] Leitgeb RA, Werkmeister RM, Blatter C, Schmetterer L. Doppler optical coherence tomography. *Progress in Retinal and Eye Research*. 2014;41:26-43
- [34] Tsai M-T, Chen Y, Lee C-Y, Huang B-H, Trung NH, Lee Y-J, et al. Noninvasive structural and microvascular anatomy of oral mucosae using handheld optical coherence tomography. *Biomedical Optics Express*. 2017;8:5001-5012
- [35] Mason C, Markusen J, Town M, Dunnill P, Wang R. Doppler optical coherence tomography for measuring flow in engineered tissue. *Biosensors and Bioelectronics*. 2004;20:414-423
- [36] Iftimia N, Ferguson RD, Mujat M, Patel AH, Zhang EZ, Fox W, et al. Combined reflectance confocal microscopy/optical coherence tomography imaging for skin burn assessment. *Biomedical Optics Express*. 2013;4:680-695
- [37] Katkar RA, Tadinada SA, Amaechi BT, Fried D. Optical coherence tomography. *Dental Clinics*. 2018;62: 421-434
- [38] Möller J, Bartsch A, Lenz M, Tischhoff I, Krug R, Welp H, et al. Applying machine learning to optical coherence tomography images for automated tissue classification in brain metastases. *International Journal of Computer Assisted Radiology and Surgery*. 2021;16:1517-1526
- [39] Maldiney T, Greigert H, Martin L, Benoit E, Creuzot-Garcher C, Gabrielle P-H, et al. Full-field optical coherence tomography for the diagnosis of giant cell arteritis. *PLoS One*. 2020;15: e0234165
- [40] Le D, Son T, Yao X. Machine learning in optical coherence tomography angiography. *Experimental Biology and Medicine*. 2021;246: 2170-2183
- [41] Tucker-Schwartz JM, Beavers KR, Sit WW, Shah AT, Duvall CL, Skala MC. In vivo imaging of nanoparticle delivery and tumor microvasculature with multimodal optical coherence tomography. *Biomedical Optics Express*. 2014;5:1731-1743
- [42] Yashin K, Karabut M, Fedoseeva V, Khalansky A, Matveev L, Elagin V, et al. Multimodal optical coherence tomography in visualization of brain tissue structure at glioblastoma (experimental study). *Современные технологии в медицине*. 2016;8:73-80
- [43] Ma X, Ji Z, Niu S, Leng T, Rubin DL, Chen Q. MS-CAM: Multi-scale class activation maps for weakly-supervised segmentation of geographic atrophy lesions in SD-OCT images. *IEEE Journal of Biomedical and Health Informatics*. 2020;24:3443-3455
- [44] Srinivasan PP, Kim LA, Mettu PS, Cousins SW, Comer GM, Izatt JA, et al.

Fully automated detection of diabetic macular edema and dry age-related macular degeneration from optical coherence tomography images.
Biomedical Optics Express. 2014;5: 3568-3577

[45] Sunija A, Kar S, Gayathri S, Gopi VP, Palanisamy P. Octnet: A lightweight cnn for retinal disease classification from optical coherence tomography images. Computer Methods and Programs in Biomedicine. 2021;200:105877